Effusion nozzle for energy-efficient NOx production in a rotating gliding arc plasma reactor

Effusion nozzle for energy-efficient NO_x production in a rotating gliding arc plasma reactor

Senne Van Alphen*[1,2], Hamid Ahmadi Eshtehardi*[1,3], Jens Bogaerts[1], Helder Van Poyer[1], James Creel[1], Marie-Paule Delplancke[3], Rony Snyders[2,4] and Annemie Bogaerts[1]

[1]Research group PLASMANT, University of Antwerp, Department of Chemistry, Universiteitsplein 1, BE-2610 Wilrijk-Antwerp, Belgium.

[2] Research group ChIPS, Department of Chemistry, University of Mons, 20, Place du parc, 7000 Mons, Belgium.

[3]Research group 4MAT, Université Libre De Bruxelles, 50 Rossevelt Av., CP 165/63, 1050 Brussels, Belgium

[4]Materia Nova Research Center, 3 Avenue Nicolas Copernic, 7000 Mons, Belgium.

* Shared first author.

E-mail: senne.vanalphen@uantwerpen.be; Hamid.AhmadiEshtehardi@uantwerpen.be; annemie.bogaerts@uantwerpen.be

Abstract

Plasma-based NO_x production is of interest for sustainable N_2 fixation, but more research is needed to improve its performance. One of the current limitations is recombination of NO back into N_2 and O_2 molecules immediately after the plasma reactor. Therefore, we developed a novel so-called "effusion nozzle", to improve the performance of a rotating gliding arc plasma reactor for NO_x production, but the same principle can also be applied to other plasma types. Experiments in a wide range of applied power, gas flow rates and N_2/O_2 ratios demonstrate an enhancement in NO_x concentration by about 8%, and a

reduction in energy cost by 22.5%. In absolute terms, we obtain NO_x concentrations up to 5.9%, at an energy cost down to 2.1 MJ/mol, which are the best values reported to date in literature. In addition, we developed four complementary models to describe the gas flow, plasma temperature and plasma chemistry, aiming to reveal why the effusion nozzle yields better performance. Our simulations reveal that the effusion nozzle acts as very efficient heat sink, causing a fast drop in gas temperature when the gas molecules leave the plasma, hence limiting the recombination of NO back into N_2 and O_2. This yields an overall higher NO_x concentration than without the effusion nozzle. This immediate quenching right at the end of the plasma makes our effusion nozzle superior to more conventional cooling options, like water cooling In addition, this higher NO_x concentration can be obtained at a slightly lower power, because the effusion nozzle allows for the ignition and sustainment of the plasma at somewhat lower power. Hence, this also explains the lower energy cost. Overall, our experimental results and detailed modeling analysis will be useful to improve plasma-based NO_x production in other plasma reactors as well.

1. Introduction

Nitrogen, the most abundant element in our atmosphere, is essential for all living organisms. About 78% of the atmosphere is made of nitrogen, but plants and animals cannot take nitrogen directly from the air. Nitrogen fixation is the process by which atmospheric nitrogen is converted to another form of nitrogen, such as ammonia (NH_3), nitric oxide (NO), nitrogen dioxide (NO_2), nitric acid (HNO_3), etc. Most of the NH_3 is industrially produced through the Haber-Bosch (HB) process. Current HB plants are tremendously optimized, with an energy consumption of 0.48 MJ/mol [1]. Despite these optimizations, the HB process uses fossil-based fuels (natural gas, oil and coal) as its energy source, as well as natural gas for H_2 production, which makes this process one of the greatest energy consumers (1-2% of the world's annual energy supply, and 3-5% of the worldwide natural gas consumption), and greenhouse gas emitters (400 Mt of CO_2 per year, accounting for 1.2% of the annual anthropogenic CO_2 emission) [2,3].

The produced gas phase ammonia from the HB process is the foundation of all nitrogen-rich fertilizers. The pressurized ammonia can directly be applied as a fertilizer into the soil, but it immediately becomes a vapor

resulting in losses of the manure and subsequently increases the human footprint in the global nitrogen cycle. One way of eliminating this manure loss is converting the volatile ammonia to involatile ammonium nitrate (NH_4NO_3) through its treatment with HNO_3 [4,5].

Recently, sustainable production of electricity through renewable energies such as wind or solar energy has grown dramatically. Electrification of the (chemical) industry is one of the key challenges of the 21st century. An upcoming technology with great potential of using renewable electricity is plasma technology, which can convert this energy into chemicals and fuels [6,7]. NO and NO_2 (i.e., NO_x) can be produced via plasma-based N_2 fixation from air, through the so-called Zeldovich mechanism:

$$N_2 + O \rightarrow NO + N$$

$$O_2 + N \rightarrow NO + O$$

Furthermore, in the presence of water vapor, i.e. moist air, the NO production is enhanced by reaction with OH radicals, through the so-called extended Zeldovich mechanism:

$$N + OH \rightarrow NO + H$$

The formed NO partially oxides into NO_2 which can then be dissolved in water to form HNO_3 through the following reaction mechanism:

$$3\ NO_2 + H_2O \rightarrow 2\ HNO_3 + NO$$

$$4\ NO + 3\ O_2 + 2\ H_2O \rightarrow 4\ HNO_3$$

This acidic solution can react with NH_3, resulting in ammonium nitrate (NH_4NO_3) production. Therefore, a fertilizer with high nitrogen content per mass (35%) can be produced [8].

Several plasma types have been explored already for NO_x synthesis; see recent overview and techno-economic analysis by Rouwenhorst et al. [9]. Birkeland and Eyde were the first to develop an industrial thermal plasma reactor for N_2 fixation [10,11], and achieved an NO production of 1-2% with an energy cost of 2.41 MJ/mol. Krop and Pollo reported an NO production of 4.7% at an energy cost of 3.5 MJ/mol, in

their electric arc plasma reactor with water injection [12]. Namihira et al. employed a pulsed arc discharge, and obtained 6.5% NO production and 4 MJ/mol energy cost [13]. Bian et al., studied NO_x production from air in a water jet discharge and reported an NO_x production of 1% with an energy cost of 47 MJ/mol [14]. Microwave (MW) plasmas at reduced pressure (50 torr) showed the highest NO production (6%) with the lowest energy cost (0.84 MJ/mol) [15]. Kim et. al., investigated the formation of NO_x from air and N_2/O_2 mixtures using a non-thermal MW plasma system, and reported 0.6% of produced NO_x with an energy cost of 3.76 MJ/mol [16]. Azizov, et al., studied the synthesis of nitrogen oxides in a non-equilibrium MW discharge and reported an NO production of 14% with an energy cost of 0.28 MJ/mol[17]. However, these record values for MW discharges, reported between 1980 and 2010, did not account for extra energy costs attributed to pumping for maintaining the low pressure regime, and were never able to be reproduced. Recently Sean et al. showed very promising results for a MW reactor working at atmospheric pressure, achieving a NO_x concentration of 3.8% at an energy cost of 2.5 MJ/mol [18]. Patil, et al., studied NO_x production in a packed bed dielectric barrier discharge (DBD) reactor with γ-Al_2O_3 catalyst, and reported 0.5% NO_x with an energy cost of 18 MJ/mol [19]. A record-low energy consumption of 0.42 MJ/mol was recently achieved by Vervloessem et al. for a pulsed plasma jet, albeit for low NO_x concentration of 0.02% [20]. In recent years, gliding arc (GA) plasmas in several designs revealed promising results. A pulsed milli-scale classical GA reactor design, studied by Patil et al. and Wang et al., showed a NO_x production of 1-2 % with energy costs between 2.8-4.8 MJ/mol [21,22]. The promising results of classical 2D GA reactors led to the development of novel 3D GA designs, aiming to improve the gas conversion and the electrode lifetime. One of these designs, the gliding arc plasmatron (GAP), studied by Vervloessem et al., achieved a NO_x formation of 1.5% at an energy cost of 3.6 MJ/mol [23]. Up until now, Jardali et al., achieved the highest NO_x production (5.2%) in atmospheric pressure plasmas, with energy cost of 2.5 MJ/mol, in a rotating gliding arc (RGA) plasma reactor [24].

While the above results look promising, an important limitation is that part of the produced NO_x in the plasma is destroyed after leaving the plasma reactor. Indeed, the temperature in the above plasma reactors

(GA or MW) reaching a typical value of 3000 K or even higher [24,25], but the gas cools down slowly after leaving the reactor. As a result, the produced NO will react with N or O atoms, back into N_2 and O_2 molecules, which reduces the overall NO_x production, as revealed by modeling [21].

Therefore, in this paper, we present a design modification to the above-mentioned RGA plasma reactor [24], by coupling it with a specific nozzle, which we call "effusion nozzle". As we will demonstrate by means of modeling, this causes a fast drop in the gas temperature when the gas leaves the reactor, thereby quenching the unwanted recombination reactions, and thus improving the overall reactor performance. We investigated the performance of this novel plasma reactor/nozzle design in a wide range of operating conditions, i.e., flow rate, input power and N_2/O_2 ratio, and we reveal the underlying mechanisms of the improvement by means of computational studies. The insights obtained by this modeling will also be useful for other plasma reactor designs.

2. Reactor setup and effusion nozzle

Figure 1 schematically illustrates the RGA plasma reactor, with details of the internal configuration, showing also the rotational gas flow behavior (black arrow line) and the arc plasma (purple) in the center (artist view), in case of steady arc mode (see below). The plasma reactor consists of a nickel cathode, supplied with high voltage, and a grounded stainless-steel anode, coupled to the newly designed effusion nozzle (see below), which acts as the reactor body (Figure 1). A spark plug (NGK BP6ES) without its ground pin is used as the powered electrode (the ground pin is replaced by the stainless-steel body of the reactor). The ceramic piece in the center of the reactor (100 mm in length, 6 mm in diameter) encloses the cathode pin so that only a cylindrical knob (1.4 mm in length, 2.5 mm in diameter) is exposed (red part in Figure 1). The reactor body comprises of a cylinder with diameter of 13 mm and length of 11.2 mm, which is followed by a cone-shape section with diameter decreasing from 13 to 4 mm. The cone-shape section extends to the outlet of the reactor, which is a cylinder of 4 mm diameter and length of 20 mm.

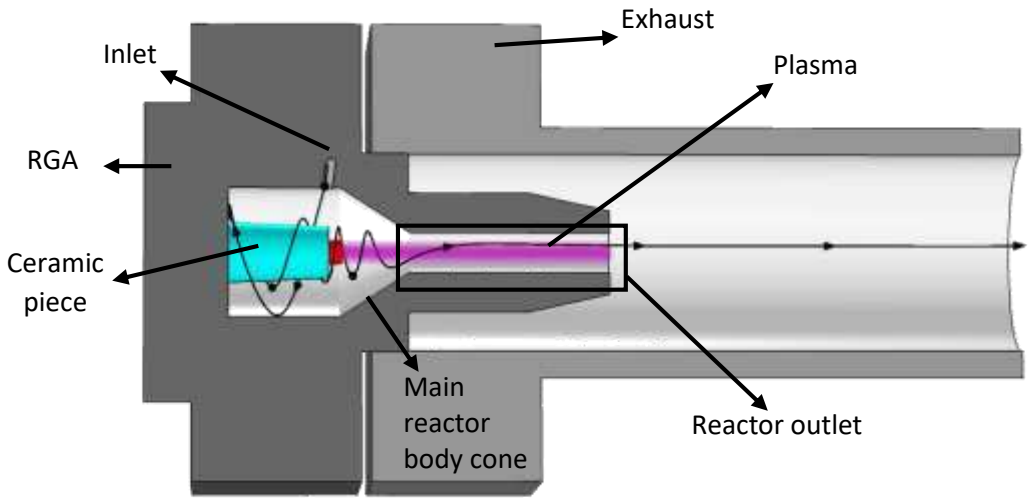

Figure 1: Schematic picture of the RGA plasma reactor, illustrating the gas flow behavior (black line) and the plasma in steady arc mode (purple zone). The cathode knob is indicated in red at the left, while the entire reactor body is at anode potential.

The (stainless-steel) effusion nozzle is coupled to the reactor outlet to enhance the reactor performance by cooling the gas temperature and quenching unwanted recombination reactions, as explained in detail by our model calculations in the results and discussions. The effusion nozzle consists of a gas-receiving cavity with inner diameter of 15 mm and length of 29.5 mm. At the end, it contains six radially distributed tiny "effusion holes" of 0.8 mm diameter, and a cuboid protruding element, called "gas divider", with 1 mm thickness, perpendicular to the axis of the gas receiving cavity; see Figure 2. The effusion nozzle screws over the plasma reactor outlet, abruptly stopping and dividing the air flow, first by the cuboid and then further by these six small radial holes. The gas divider, indicated in red color in Figure 2, serves as anchor for the arc. A stainless-steel cylinder with diameter and length of 25 mm and 295 mm, respectively, is coupled to the whole system to collect the exhaust gas stream and to provide connection to the gas diagnostic device.

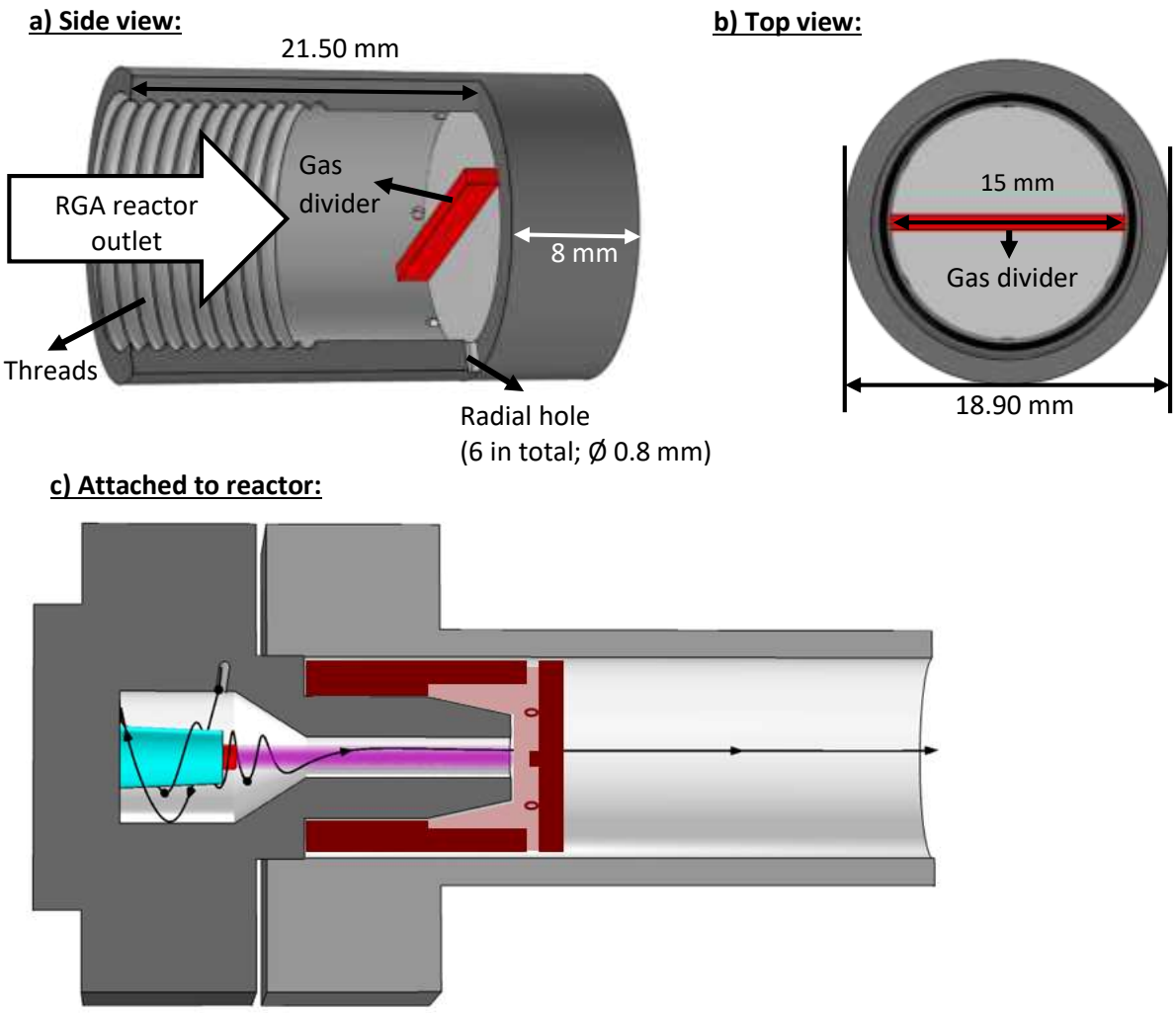

Figure 2: Schematic picture of the effusion nozzle with dimensions, in side view (a), top view (b) and attached to the reactor (c). In the latter case, the nozzle is colored in red. The gas divider (red bar in (a) and (b)) serves as anchor when the effusion nozzle is mounted on the RGA, and it has a width of 1 mm, height of 2 mm, and length of 15 mm. It sits on top of the 8 mm steel back wall, across the whole nozzle.

The arc plasma is ignited using a 10 kV DC power supply (Topower TN-XXZ02). A 25 kΩ ballast resistor is connected to the circuit to compensate for changes in the discharge current and to prevent over-heating of the power supply, allowing for a maximum current of 280 mA. A high voltage probe (TESTEC 1000:1)

measures the discharge voltage, while the current is measured from the voltage drop across a 25 Ω resistor. An oscilloscope (Keysight DSOX1102A, 70 MHz bandwidth, 2 GSa s^{-1} sample rate) is utilized to record the time evolution waveform of the discharge voltage and current.

N_2 and O_2 feed gases (99.999% purity) are mixed and injected to the system through a tangential inlet of 1 mm diameter (see Figure 1). The gas volumetric flow rates are adjusted using mass flow controllers (Bronkhorst F-201CV). In the main RGA reactor body, a reverse vortex flow is created due to the tangential gas inlet and the shape of the reactor. As illustrated by the black line in Figure 1, the gas first swirls upwards along the reactor wall, before collapsing into a smaller inner vortex that flows around the ceramic piece and towards the reactor outlet.

We measured the total produced NO_x as sum of the NO and NO_2 concentrations (%) in the exhaust stream, by a non-dispersive infrared sensor along with an ultraviolet sensor, for quantitative analysis of the species concentrations (EMERSON-Rosemount X-STREAM enhanced XEGP continuous Gas analyzer). N_2O and N_2O_5 are only formed in the ppm range, and therefore do not contribute to the NO_x concentration in a significant way. This is in agreement with our previous studies [24].

The average plasma power (P) is calculated by

$$\mathrm{P[W]} = \sum_{j=1}^{N} \frac{V_j I_j}{N} \tag{1}$$

Where I_j and V_j are the recorded discharge current and voltage, respectively, and N is the number of records.

Knowing the plasma power and the total measured NO_x concentration, we define the energy cost of the process as:

$$\text{Energy cost [MJ/mol]} = \frac{\mathrm{P[J/s]} \times 24\mathrm{[L/mol]} \times 60\mathrm{[s/min]} \times 100\mathrm{[\%]}}{C_{NO_x}\mathrm{[\%]} \times \mathrm{Q[L/min]}} \times 10^{-6} \tag{2}$$

Where 24 L/mol is the molar volume at the reactor inlet (1 atm and 293.15 K), Q is the total gas volumetric flow rate, and 10^{-6} is the conversion factor from J to MJ.

We performed measurements in a wide range of operating conditions, i.e., volumetric flow rates ranging from 1 to 10 L/min, electrical currents from 60 to 200 mA, and N_2/O_2 ratios ranging from 0.25 to 4. Details are given in Supporting Information (SI; section S.1.1). All experiments were performed three times for each of the conditions, and the average values are taken over a 5-minute measurement period. A 5-minute time period is sufficient, as the NO_x concentration in the RGA's effluent quickly reaches a stable value, which is demonstrated by the time evolution of the measured NO_x concentration, shown in figure S.1 in the SI (Section S1.2). The reported values are the weighted averages, and the error bars are calculated based on the standard deviation of the results of each experiment from its corresponding average value. More information about the experimental procedure, diagnostic device specification and calibration is given in the SI (Section S.1.2).

3. Model description

We developed four complementary models to describe the gas flow, plasma temperature and plasma chemistry, aiming to reveal the mechanisms responsible for the better performance of the RGA with effusion nozzle. These models include (i) a turbulent gas flow model, (ii) a fully coupled heat transfer model, (iii) streamline integration, and (iv) a quasi-1D plasma chemistry model.

Figure 3 illustrates how these four models are solved sequentially, with the output of one model serving as input for the next. First, a turbulent gas flow model calculates the gas flow behavior inside the reactor. Second, a fully coupled heat transfer model is solved, which calculates the gas heating and heat transfer in the reactor by describing the arc as an analytical heat function. This model recalculates the gas flow behavior, because the gas heating by the plasma influences the gas flow behavior, which was not accounted for in the initial turbulent gas flow model. Subsequently, the adjusted gas flow behavior and temperature profile are used as input for streamline integration simulations, which describe the trajectory of gas molecules, and provide a record of the gas temperature and power density "felt" by these gas molecules as they flow through the plasma towards the outlet. This gas temperature and power density profile is then used as an input into a quasi-1D plasma chemical kinetics model, which simulates the plasma chemistry of

the N_2/O_2 mixture, and calculates the NO_x concentrations and energy cost of the conversion process. This combination of models is an improved version of our models presented before [28]. In the following sections, we briefly describe each model in the order in which they are solved. A more detailed description is given in SI (section S.2).

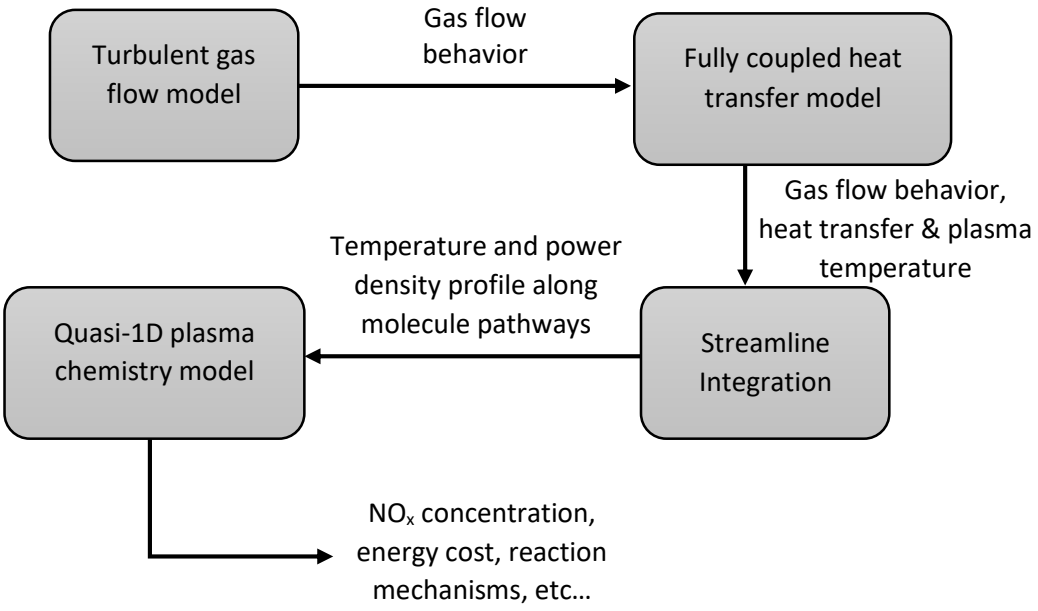

Figure 3: Overview of the four complementary models, their inputs, outputs and how they complement each other.

3.1. 3D Turbulent gas flow model

We described the gas flow behavior with a turbulent gas flow model, using the computational fluid dynamics (CFD) module in COMSOL Multiphysics version 5.6. There is a high level of turbulence in the RGA reactor, due to its somewhat complex geometry involving the effusion nozzle and because it operates at high internal flow speed (66 m/s at the inlet for a 2 L/min flow rate). Therefore, instead of solving the Navier-Stokes equations in their full form, which is computationally intensive, we used the Reynolds-averaged-Navier-Stokes (RANS) Menter's shear stress transport (SST) [29] turbulence model. The RANS model leads to a significant reduction in computation time, as it averages all fluctuating turbulent quantities

over time, and the SST model improves accuracy as it combines the common k-ε model in the free stream with the more accurate k-ω model near the walls [29]. More information about this model is given in the SI (section S.2.1).

3.2. Fully coupled heat transfer model

The gas heating in the plasma arc is simulated by adding a heat source in the shape of the arc to the 3D turbulent gas flow model, described in previous section. To provide a realistic heating profile, the gas heating provided by the plasma is calculated using the measured plasma power minus the power needed to produce the measured NO_x concentration. Indeed, the formation of NO and NO_2 is endothermic and thus also requires power, which is thus not available anymore for gas heating. The details of this approach, which is also significantly different from our previous model [28], are given in SI (section S.2.2). A sensitivity analysis of the heating profile is also provided in this section of the SI.

Using the heating profile of the arc, the gas temperature is then calculated by solving the thermal balance equation for the gas flow, but also for the solid domains (ceramic and metal parts) of the reactor. In this way, we account for the convective heat transfer inside the reactor, the conductive heat transfer within the solid parts of the reactor and the convective and radiative heat transfer towards the environment. Furthermore, we solved again a turbulent gas flow model, simultaneously with this thermal balance equation, because the gas temperature affects the flow behavior, hence the name "fully-coupled heat transfer model". This turbulent gas flow model is the same as described above, except that now the influence of the temperature on the gas density and viscosity is accounted for. More information about this fully coupled model is given in the SI (section S.2.2-S2.4).

3.3. Streamline integration

We cannot describe the full chemistry within the above 3D models, as this would make them too computationally intensive. Therefore, we used a quasi-1D plasma chemical kinetics model to reveal the chemical pathways and calculate the NO_x yields. For this purpose, we need the gas temperature and power

density experienced by the gas molecules as input. Therefore, we integrated the gas streamlines, calculated by the fully coupled heat transfer model, over time, yielding the trajectory of the gas molecules in the reactor. During this integration, the model records the gas temperature and power density, which is experienced by the gas along the trajectory when flowing through the plasma towards the outlet. We used the particle tracing module within COMSOL Multiphysics 5.6 to simulate this gas molecule flow behaviour, and we calculated the trajectory path length q by:

$$q = \int_0^{t_{outlet}} v \, dt \qquad (3)$$

$$v = \sqrt{{v_x}^2 + {v_y}^2 + {v_z}^2} \qquad (4)$$

Here, v_x , v_z, and v_y are the gas flow velocities in x, y and z direction, and t_{outlet} is the time needed for the gas to flow to the outlet.

When we assume that chemical species follow these gas flow trajectories, we only consider the convection of molecules due to the turbulent gas flow, thus neglecting transport by diffusion and migration of charged particles. Because of the high velocity in the vortex flow, convection is indeed the most important mode of transport for all chemical species, justifying this assumption.

In total, we integrated 10,000 streamlines to represent the flow behavior. The contribution of each streamline to the total flow is defined by the mass flow $\dot{m}$ along each streamline, defined by:

$$\dot{m} = v \, \rho \, A \qquad (5)$$

Where v is the gas flow velocity defined in equation 4, ρ is the gas density and A the cross sectional area of the tubular region of fluid surrounding the streamline, often referred to as a streamtube. This would provide 10,000 possible trajectories as input for the quasi-1D chemistry model. However, many streamlines can be grouped together, as they experience similar conditions. Therefore, we grouped the streamlines based on a similar maximum temperature, and we calculated the average trajectory of each group. As a result, we

reduced the 10,000 possible trajectories to only 11 averaged trajectories, which were then used as input for the quasi-1D plasma chemistry model.

3.4. Quasi-1D plasma chemical kinetics model

A quasi-1D chemical kinetics model can describe an extensive plasma chemistry within a reasonable calculation time, as it ignores most of the spatial variations, i.e. diffusion and migration. Therefore, it is a powerful tool for revealing chemical formation pathways and calculating NO_x concentrations. When all spatial variations are neglected (i.e., uniform plasma), this modelling approach is commonly called 0D or global model. However, we used the gas velocity to convert the time-evolution of the simulation into a spatial variation (i.e., following the path of the gas molecules); hence the name "quasi-1D" model.

We developed this model with the zero-dimensional plasma kinetics solver ZDPlasKin [30]. It calculates the density change of all chemical species as a function of time by solving a continuity equation for all species, accounting for the production and loss terms defined by the chemical reactions. More details about this model can be found in the SI (section S.2.3)**.**

We took into account 43 different species (see Table 1) which react in 1,214 electron impact reactions, 481 ionic reactions, 432 neutral reactions. Plasma-wall interactions were not incorporated because the vortex swirl flow isolates the plasma from the reactor wall to improve electrode lifetime. The reactions, rate coefficients, and references where these data were adopted from, can be found in Ref. [23]. Note that the chemical kinetics model in this work does not incorporate the vibrational kinetics that are described in Ref. [23], as our RGA is a quasi-thermal" or "warm" plasma in which the gas temperature exceeds 3000 K. In this temperature range vibrational-translational relaxation collisions occur fast enough so that vibrational excitation of N_2 and O_2 does not play a significant role in the NO_x formation process [31].

Table 1:Plasma species included in the model.

Neutral species	**Radicals**	**Charged species**	**Excited species**
N_2, O_2, O_3, NO, NO_2, N_2O, NO_3, N_2O_3, N_2O_4, N_2O_5	N, N(2D), N(2P), O, O(1D), O(1S)	e^-, N^+, N_2^+, N_3^+, N_4^+, O^-, O_2^-, O_3^-, O_4^-, O^+, O_2^+, O_4^+, NO^+, NO_2^+, N_2O^+, NO^-, NO_2^-, N_2O^-, NO_3^-, $O_2^+N_2$	$N_2(A^3\Sigma_u^+)$, $N_2(B^3\Pi_g)$, $N_2(C^3\Pi_u)$, $N_2(a'^1\Sigma_u^-)$, $O_2(a^1\Delta)$, $O_2(b^1\Sigma^+)$, $O_2(A^3\Sigma^+, C^3\Delta, c^1\Sigma^-)*$

As mentioned above, the streamline integrations provides 11 averaged temperature and power density profiles for the RGA reactor, which are used as input in this quasi-1D plasma chemistry model. We calculated the underlying chemistry and NO_x concentrations of each of the groups, and we obtained the overall NO_x concentration by calculating the weighted average of all 11 groups, where the weights are

represented by the ratio of the particles present in one group over the total number of particles of all 11 groups combined.

4. Results and discussion

4.1. Improvement in NO_x yield and energy cost due to the effusion nozzle

Figure compares the performance of our reactor with and without the effusion nozzle, in terms of NO_x concentration (i.e. $NO + NO_2$), energy cost and supplied plasma power. As explained in the SI (section S.3), our RGA reactor operates in three distinct regimes: (i) rotating arc mode at low power (90-130 W) where the arc rotates/glides along the reactor body, (ii) transition regime at intermediate power (135-185 W), and (iii) steady arc mode at power above 185 W, where the arc is stabilized due to the intense heat transfer to the reactor walls (so-called wall stabilization), and elongates until it reaches the furthest point of contact on the reactor outlet (schematically illustrated in Figure 1 above). In the last case, it remains there in a stable regime in the center of the reactor with constant length, and fills most of the reactor outlet, such that all of the incoming gas effectively passes through the plasma. Figure 4 shows the results for both rotating and steady arc regime, in a wide range of N_2/O_2 ratios.

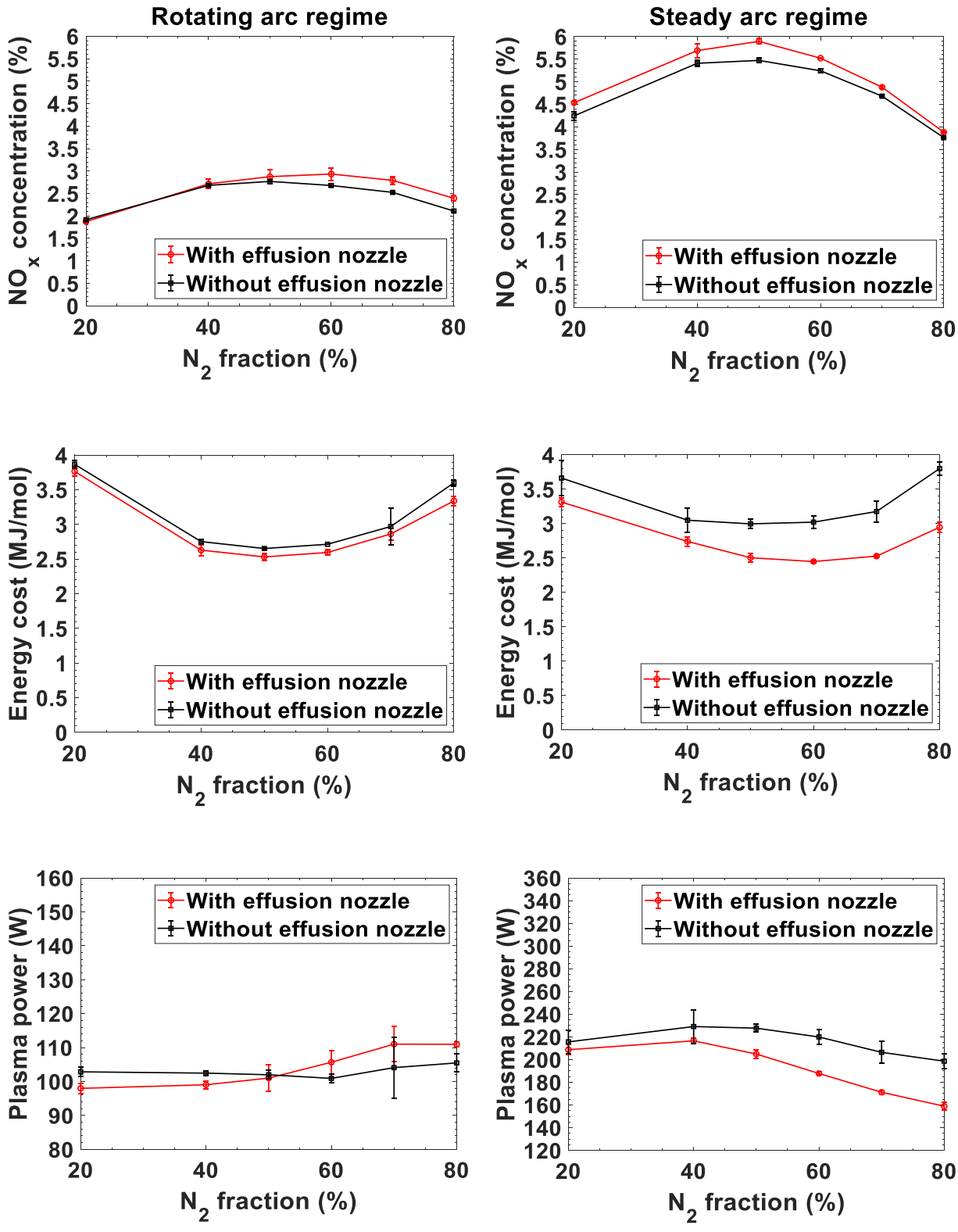

Figure 4. Measured NO_x concentration (a, b), energy cost (c, d) and plasma power (e, f) in the RGA plasma reactor operating with and without the effusion nozzle, as function of N_2/O_2 ratio, in rotating (left) and

steady (right) arc regimes. The applied current in the rotating arc regime was between 60 and 120 mA, while it was between 120 and 200 mA in the steady arc regime. The total flow rate was fixed at 2 L/min.

In the rotating arc regime, for N_2/O_2 ratios below 50/50, the effusion nozzle allows ignition and sustainment of the plasma arc at lower power values than without nozzle (Figure e), reaching about the same NO_x concentration (Figure a). For N_2/O_2 ratios above 50/50, slightly higher power should be supplied as without nozzle, but higher NO_x concentrations are achieved. The effect of either lower power (for the same NO_x concentration) or higher NO_x concentration yields a slightly lower energy cost for each N_2/O_2 ratio, with on average 4.5% improvement, and the largest improvement of 7.3% for an N_2/O_2 ratio of 80/20, mimicking dry air composition (Figure c).

In the steady arc regime, a lower power can sustain the arc across the entire range of N_2/O_2 ratios when it is operating with the effusion nozzle (Figure f). Moreover, the effusion nozzle also results in slightly higher NO_x concentrations (improvements up to 8%) (Figure b). As a consequence of both, the energy cost with the effusion nozzle drops on average by 16.3% over the entire range of N_2/O_2 ratios compared to without nozzle, with the largest improvement of about 22.5% at N_2/O_2 ratio of 80/20. Overall, our best results are obtained in the steady arc regime, at an N_2/O_2 ratio of 50/50, yielding a NO_x concentration of 5.9%, at an energy cost of 2.5 MJ/mol, but an N_2/O_2 ratio of 60/40 yields an even slightly lower energy cost of 2.4 MJ/mol.

As predicted by our models, only NO is initially formed in the plasma, as NO_2 is destroyed at these high gas temperatures. Once out of the plasma, part of the formed NO oxidizes to NO_2 when the gas has cooled down. By the time the gas reaches our detector, the gas consists of both NO and NO_2. Across the different gas mixtures, the NO/NO_2 ratio varies from 0.2 (at a N_2/O_2 ratio of 20/80) to 0.9 (at a N_2/O_2 ratio of 80/20), hence yielding a higher NO_2 concentration when more O_2 is present in the mixture.

We also evaluated the performance of our RGA reactor with the effusion nozzle in a wide range of operating conditions, i.e., not only the N_2/O_2 ratio and power (Figure 4), but also in a wide range of gas flow rates from 1 to 10 $L.min^{-1}$. The effect on the NO_x concentration, energy cost and corresponding plasma power as

a function of N_2/O_2 ratio is presented in SI (section S.3.2; Figure S.7). The best results for the rotating arc regime were obtained for an N_2/O_2 ratio of 50/50 at 1.5 L/min, reaching an NO_x concentration of 4.5% (Figure S.7a), at an energy cost down to 2.1 MJ/mol (Figure S.7c),. The best results for the steady arc regime were reached for an N_2/O_2 ratio of 50/50 at 1L/min, reaching an NO_x concentration of 6.1% (Figure S.7b), at an energy cost down to 2.7MJ/mol (Figure S.7d).

It can be argued that our obtained energy costs are not yet competitive with the combined HB and Ostwald process. Indeed, Rouwenhorst et al. [9] performed a techno-economic analysis, and reported that the energy cost of plasma-based NO_x production must be reduced to 0.7 MJ/mol in order to compete with the industrial HB and Ostwald process. Hence, further efforts will be needed to improve the performance. Nevertheless, from an environmental point of view (reduction of human footprint), plasma-based NO_x production has massive potential for distributed production plants based on renewable electricity by simply using air as feed gas. Additionally, no CO_2 is produced in this process in contrast to the conventional HB process, which produces 1.9 metric tons of CO_2 per metric ton of NH_3 [6,32].

4.2. Underlying mechanisms of the improvement: Insights from the models

To explain the improved performance due to the effusion nozzle, we first discuss for both configurations (i.e. with and without the effusion nozzle) the gas flow behavior, arc shape, and temperature profile, as calculated by the fully coupled heat transfer model. Next, we will analyze the molecule trajectories of the streamline integrations and organize them based on their maximum experienced temperature into 11 temperature groups. Finally, we will analyze the obtained NO_x concentrations and reaction rates from each of the temperature groups.

We only show this detailed analysis for the RGA in the steady arc regime, as it yields the best performance, and we will focus on the N_2/O_2 feed ratio of 80/20, which closely mimics dry air, as it is of most interest for practical applications.

4.2.1. Gas flow behavior

Figure 5(a,b) illustrates the gas flow behavior in the RGA with and without the effusion nozzle, showing a complex rotational flow pattern inside the reactor. The gas enters the reactor via the tangential gas inlet at a large initial flow velocity of ~60 m/s. Upon entering the main reactor body, the gas velocity drops to ~30 m/s and starts to flow upward along the reactor wall, further decreasing in speed to ~10 m/s. When the gas has reached the top, it will collapse into a smaller inner vortex and flow along the ceramic piece towards the reactor outlet, where the vortex behavior quickly disappears.

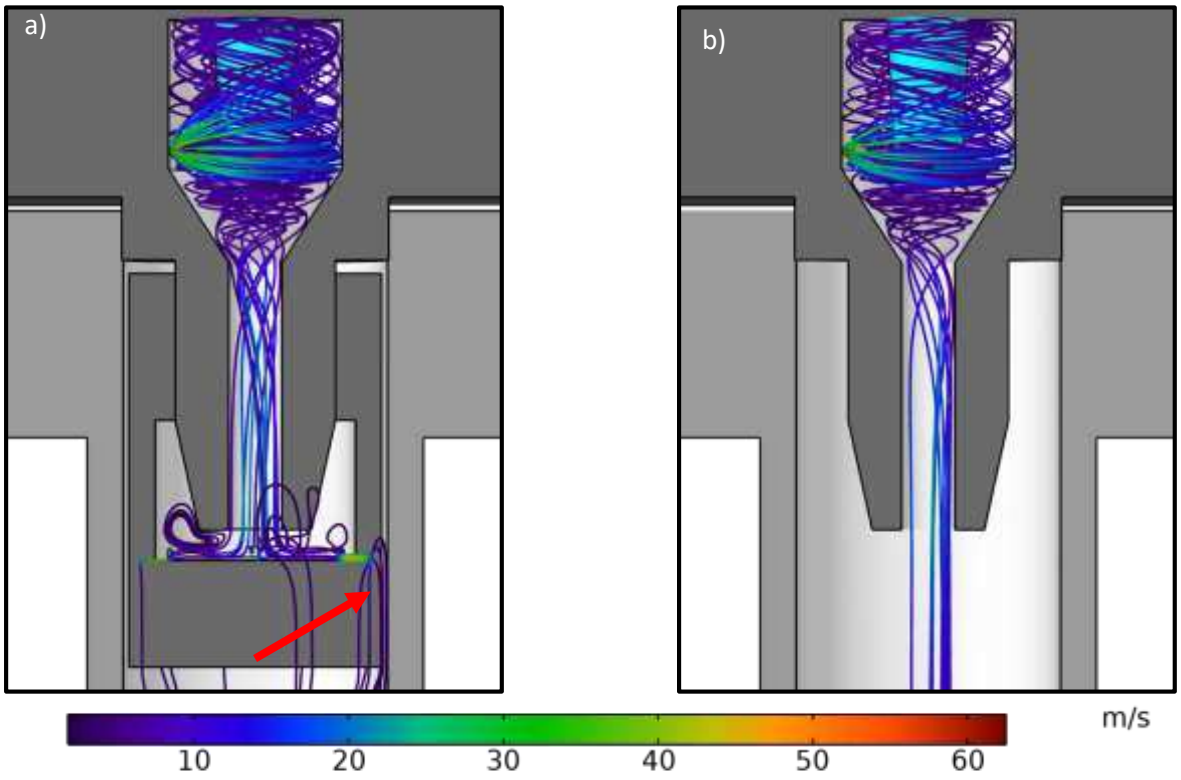

Figure 5: Calculated gas flow streamlines for the RGA with (a) and without (b) the effusion nozzle. The color scale denotes the gas velocity.

Up to this position, the flow behavior is the same for the RGA with and without the effusion nozzle. However, the flow in the lower part of the outlet is largely influenced by the nozzle; see Figure 5. More specifically, the gas flow is blocked and needs to flow through the small radial holes inside the nozzle to reach the exhaust. Figure S.9 in SI (section S.4) shows a close-up of the gas flow behavior inside the

effusion nozzle. The gas spreads in all directions upon leaving the reactor outlet, because the nozzle blocks the original flow path. The flow does not immediately exit the nozzle through the small radial holes, and some recirculation can occur (see Figure S.9). When the gas passes through the small radial holes, it shortly accelerates to ~45 m/s, and immediately decelerates to velocities below 10 m/s when it has passed the small holes; see red arrow in Figure 5.

4.2.2. Temperature profile

Figure 6 shows the temperature profile with and without the effusion nozzle, calculated based on the measured plasma power as input in the model. As observed in Figure 4, the plasma power for the 80/20 N_2/O_2 feed ratio was 159 W for the effusion nozzle and 199 W for the set-up without the nozzle. The resulting temperature profiles are compared in Figure 6(a) and 6(c). We observe two differences. First, we see very fast cooling in the effusion nozzle, cf. the fast transition of red to blue in Figure 6(a). This demonstrates that quenching occurs in the set-up with the effusion nozzle, and that it can possibly affect the chemistry (see further). Second, we see that the setup without nozzle exhibits a higher maximum gas temperature inside the plasma region (i.e., 5129 K vs 4615 K), which is of course due to the higher power causing more heating. Therefore, we also compare the temperature profile with and without the effusion nozzle calculated with the same plasma power of 159 W (Figure 6(a,b)). Although this simulation does not represent the experimental conditions, it removes the influence of the higher power (and thus temperature) for the RGA without the effusion nozzle, and allows us to see whether quenching affects the temperature inside the arc as well. The maximum temperature inside the arc is now the same, so it is clear that the effusion nozzle only causes very fast cooling when the gas arrives at the wall of it, and escapes through the small holes.

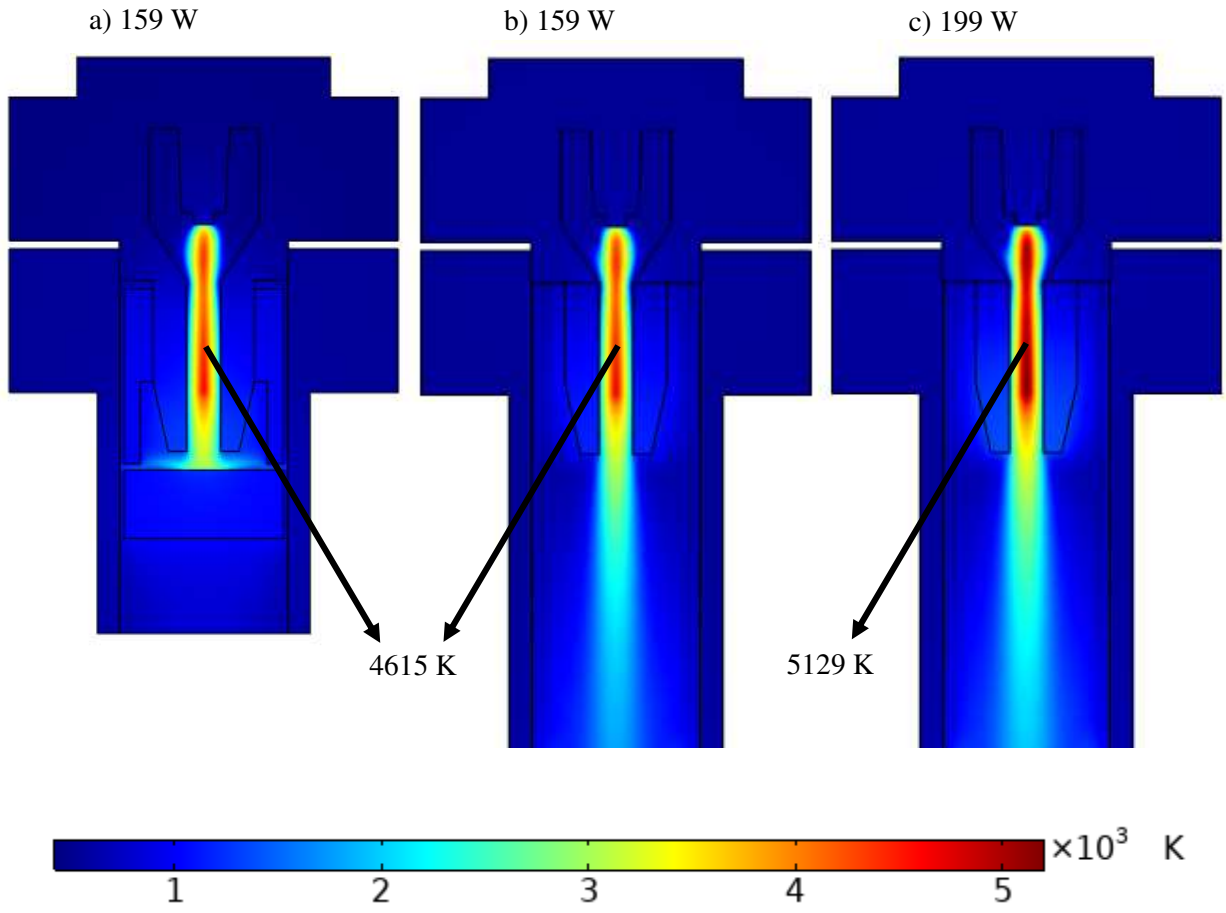

Figure 6: Calculated temperature profiles, with the effusion nozzle based on the measured plasma power of 159 W (a), without the effusion nozzle using the same power (b), and using the measured power of 199 W (c).

4.2.3. Gas flow trajectories

Because of the non-uniform temperature profile in the reactor outlet, with a maximum in the center and decreasing towards the walls (cf. Figure 6), the gas molecules will feel a different temperature when flowing through the reactor, depending on their exact trajectory. This is illustrated in Figure S.9 of the SI (section S.4), where it is clear that molecules flowing closer to the center of the reactor outlet experience a higher temperature than molecules flowing near the walls.

As explained in section 3.3, we grouped all molecules/trajectories into 11 different groups, based on the maximum experienced temperature during their trajectory. Figure 7 presents a histogram with the fraction of gas molecules in each group for the three different cases of Figure 6 (i.e., with the effusion nozzle and measured plasma power of 159 W, and without nozzle, for the same power, and for the measured power of 199 W).

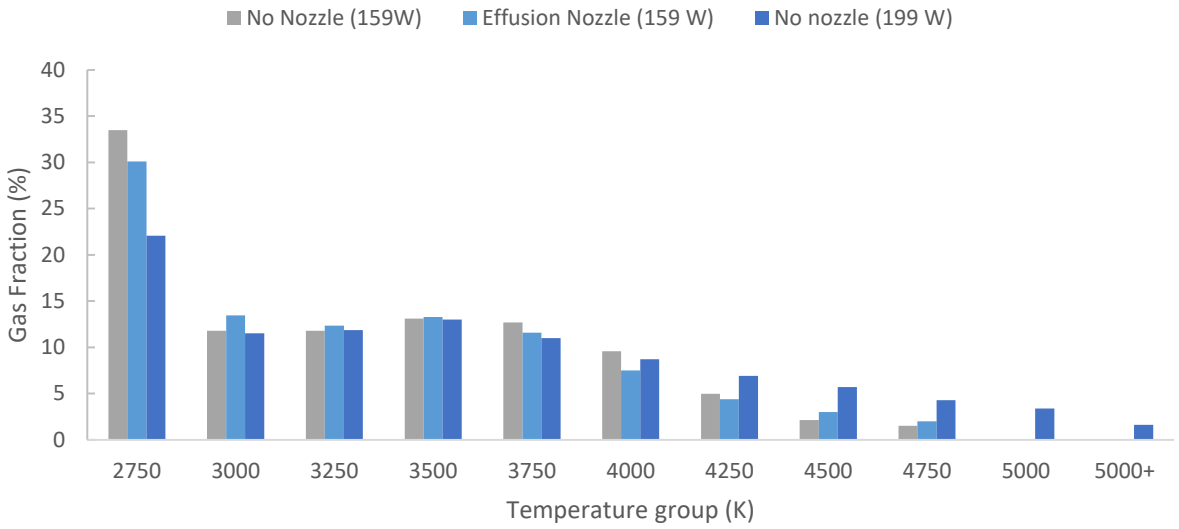

Figure 7: Calculated gas fraction in the 11 temperature groups, with and without the effusion nozzle, at the measured plasma power (159 W with, and 199 W without nozzle), as well as without nozzle, for the same power of 159 W. The values in the x-axis denote the maximum of each temperature group (except for the last group).

This figure shows that for all three cases the fraction of gas populating each temperature group roughly decreases as the temperature increases. This is attributed to the fact that the highest gas temperatures are found in the center of the plasma (cf. figure 6), which covers only a small volume of the reactor. Furthermore, due to the high gas temperatures, the gas density also decreases towards the hot center of the plasma. The fact that higher gas temperatures are achieved for the higher power case of 199 W, is also represented in this figure, as the distribution indicates that 5% of the gas experiences temperatures higher than 5000 K for the 199 W case, while both the 159 W cases (with and without effusion nozzle) don't reach

these high temperatures. The figure also shows that for a reactor with and without nozzle (both 159 W cases), the difference in experienced temperatures are only minimal.

4.2.5. NO_x formation

The calculated NO_x concentrations for the 11 temperature groups, obtained from running the quasi-1D chemical kinetics model for each of these groups, are plotted in Figure 8. It is clear that the NO_x formation strongly depends on the temperature experienced by the molecules. For gas molecules that experience temperatures below 3250 K, barely any NO_x formation occurs. Hence, only the higher temperature groups, which are found closer to the center of the plasma, contribute to the overall NO_x concentration. In these zones both the gas temperature and electron temperature are very high, i.e. more than 4000 K and ±1 eV respectively, yielding local high NO_x concentrations up to 10%. Note that these electron temperatures are locally high enough to induce significant NO_x formation. When we compare the NO_x formation with and without the effusion nozzle, we see that the reactor with the effusion produces slightly higher NO_x concentrations in the 3500-4750 K groups. This indicates that the effusion nozzle clearly affects the chemistry (see next section). Finally, the figure shows that the higher plasma power (199 W instead of 159 W) does not really affect the NO_x formation within each group for the configurations without nozzle (see also next section).

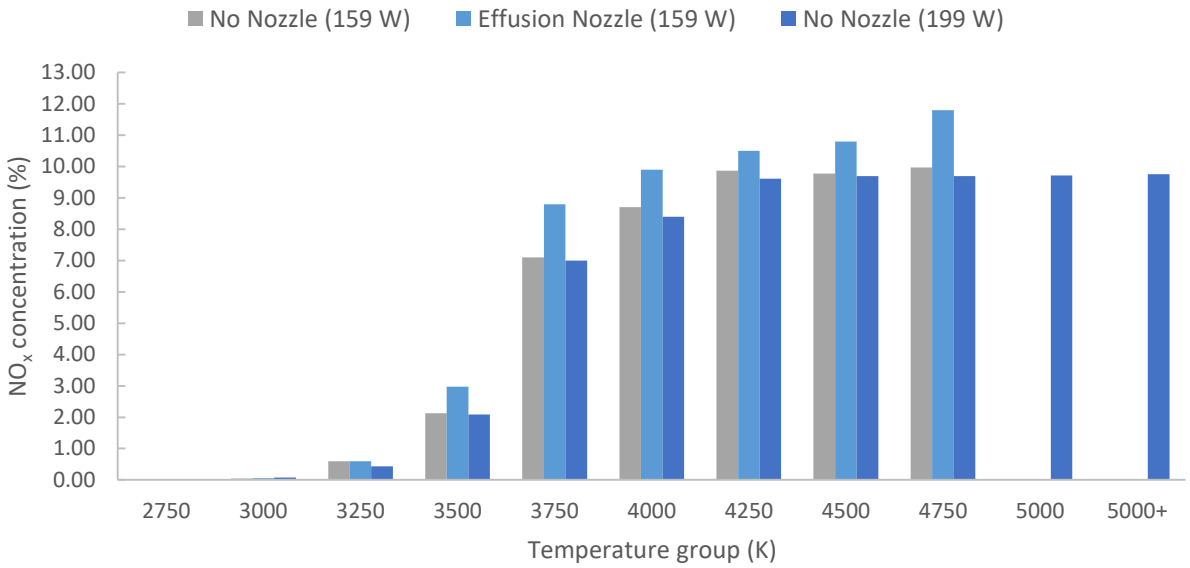

Figure 8: Calculated NO_x concentration in the 11 temperature groups, with and without the effusion nozzle, for the same cases as in Figure 7.

To calculate the overall NO_x concentration for each configuration, we multiplied the gas fraction from each temperature group (Figure 7) with its corresponding NO_x concentration (Figure 8), and took the summation over all 11 groups. The results are shown in Table 2, and they are compared with the measured NO_x concentrations.

Table 2: Summary of the experimental and calculated overall NO_x concentration, with and without the effusion nozzle. The experimental data are obviously only given at the measured plasma power, while the calculations without nozzle were performed both for the measured plasma power (199 W) and the same plasma power as with nozzle (159 W), for a theoretical comparison.

Plasma power	NO_x concentration (%) without nozzle		NO_x concentration (%) with effusion nozzle	
	Experimental	Model	Experimental	Model
159 W	/	2.76	3.88 ± 0.01	3.30
199 W	3.77± 0.02	3.95	/	/

First, to evaluate whether quenching affects the overall formed NO_x concentration, we compare in Table 2 the overall concentration with and without nozzle, calculated at the same plasma power (159 W). The concentration with the effusion nozzle is higher than without (3.30% vs. 2.76%). As both configurations show a similar gas fraction distribution over the different temperature groups (see Figure 7), the higher overall NO_x concentration with the effusion nozzle is clearly due to the larger NO_x formation in the higher temperature groups, especially in the group above 3500 K (see Figure 8). This is indeed due to the quenching, as explained in next section.

Second, Table 2 shows that the higher plasma power (199 W vs. 159 W) for the configuration without effusion nozzle results in a higher overall NO_x concentration (3.95% vs. 2.76%), due to the higher temperature, enhancing the chemistry.

Last but not least, we see that the model underestimates the overall NO_x concentration with the effusion nozzle. This is probably attributed to the heat source approximation made in the model, i.e., based on the plasma power minus power used for the chemistry, and not accounting for details, like local power density hot spots near the cathode and anode of the reactor. As a result, our simulations show lower temperatures in these regions than would be expected in reality, thus potentially leading to an underestimation of the achieved NO_x concentration. Indeed, the calculations are quite sensitive to small changes in temperature (due to the temperature dependence of all rate coefficients). We could “tune” our calculations until better quantitative agreement with the experiments is achieved, but we believe this would not bring more physical

insight. We prefer to keep the modelling strategy entirely transparent, and we believe the agreement is good enough to explain the observed improvement due to the effusion nozzle; see next section.

4.2.6. Reaction rate analysis

It is clear from Figure 8 that the higher temperature groups determine the NO_x formation. Hence, to understand why the effusion nozzle enhances the NO_x formation in these higher temperature groups, we plot in Figure 9 the change in NO_x concentration as a function of time for the gas molecules in the 3750 K temperature group, with and without the effusion nozzle. We only discuss the details for this temperature group, as a representative example, because the same behavior was observed for the other temperature groups.

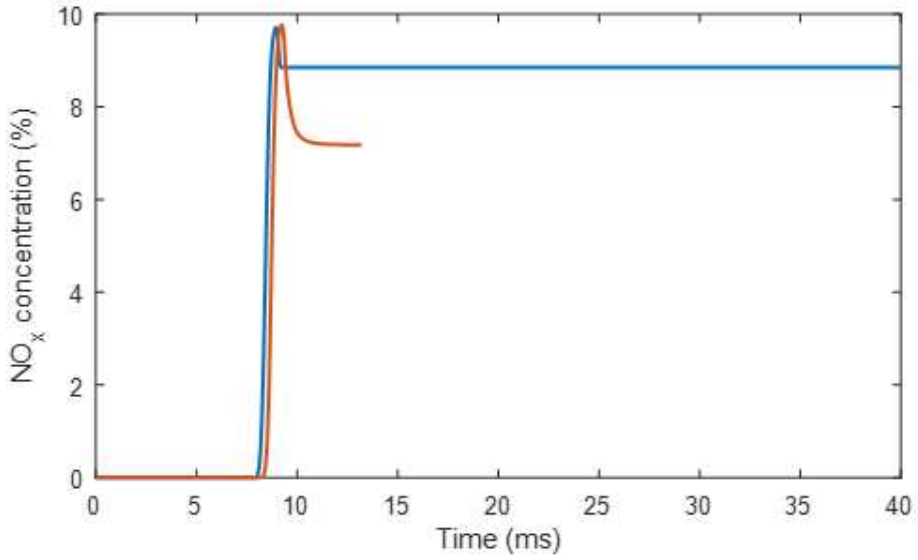

Figure 9: Calculated NOx concentration in the 3750 K temperature group as a function of time, with (blue) and without (orange) the effusion nozzle.

First of all, the difference in time scale between both reactor configurations is because the effusion nozzle blocks the flow path of the gas when it exits the reactor outlet (see Figures S.6 and S.7 in SI; section S.4), such that the gas takes longer to reach the exhaust due to recirculation inside the effusion nozzle before it flows through the radial holes. Next, the small offset between both peaks in NO_x concentration is because

the molecules flow a little longer in the vortex of the main reactor body without the effusion nozzle. This small difference is however not significant and was not the result of changing anything in the reactor body geometry. Furthermore, the time spent in the plasma was the same for both configurations, and thus the offset has no effect on the model outcome.

It is clear from Figure 9 that both with and without the effusion nozzle, the NO_x concentration first rises to a similar value, due to the NO_x formation inside the plasma, but then the concentration drops when the gas leaves the plasma, until it stabilizes to a constant value, which is clearly higher with than without effusion nozzle.

Indeed, the NO_x concentration without the effusion nozzle drops more significantly, and this can be explained by reaction analysis of the most important formation and destruction reactions (see details in SI, section S.5; Table S.4). From this analysis, it is clear that the drop in NO_x concentration is due to the backward reactions of the Zeldovich mechanism, which convert NO back into N_2 and O_2:

$$N + NO \rightarrow O + N_2 \quad (6)$$

$$O + NO \rightarrow N + O_2 \quad (7)$$

These reactions reduce the overall NO_x concentration if the rates of the destruction reactions (as written in eq. (6) and (7)) are higher than the formation rates of NO; i.e. the Zeldovich mechanism (reverse of eq. (6, 7)). Therefore, we plot the sum of both formation and destruction reactions (i.e., forward and backward reactions of the Zeldovich mechanism) as a function of time in Figure 10. We also plot the average gas temperature profile experienced by these molecules (in the 3750 K group) to explain the behavior seen in Figure 9. We are not interested in the time before the plasma, which is when the gas enters the RGA reactor and circulates upwards. Some chemistry can already occur, but it is negligible compared to the conversion in the plasma (cf. the log scale in Figure 10, and see also Figure 9: significant NO_x formation only starts around 7-8 ms).

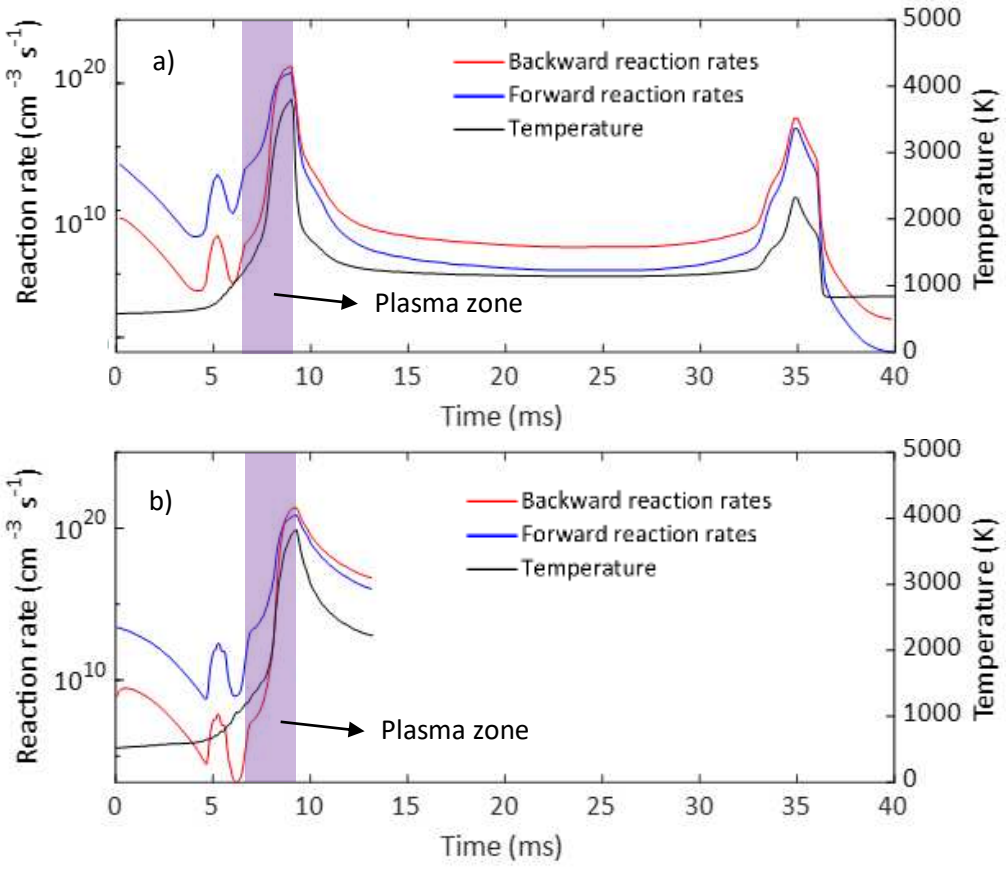

Figure 10: Calculated total forward and backward reaction rates of NO formation/destruction as a function of time, with (a) and without (b) the effusion nozzle, for the 3750 K temperature group. The black curve is the gas temperature, and the purple region is the plasma zone. Note that the gas takes longer to reach the exhaust in the case of the effusion nozzle (a), as it experiences some recirculation inside the effusion nozzle before it flows through the radial holes.

For the RGA with the effusion nozzle (Figure 10a), the reaction rates for both forward and backward reactions rise upon rising temperature when the gas passes through the plasma, but the total forward reaction rate is higher than the total backward reaction rate, thus resulting in net NO_x formation (see Figure 9). When the gas reaches the maximum temperature at the end of the plasma, the rates of both total forward and

backward reactions also reach their maximum, and they are equal to each other, hence leading to no further NO_x formation, explaining the maximum NO_x concentration in Figure 9 at this time point.

When the gas exits the plasma, the temperature drops quickly, because the effusion nozzle acts as heat sink (see Figure 6). Hence, both forward and backward reaction rates drop quickly, but the total backward reaction rate is slightly higher than the total forward reaction rate, explaining the drop in NO_x concentration of Figure 9. However, this drop is limited, because the quenching due to the effusion nozzle (fast drop in temperature) leads to such a fast drop in reaction rates that after 2 ms they are already low enough to not influence the NO_x concentration further, explaining why the latter remains constant until reaching the exhaust (see Figure 9).

Note that after this fast cooling, the molecules recirculate in the effusion nozzle, characterized by lower temperatures, and the reaction rates stay low. However, as seen in Figure 10a, the molecules feel a second peak in temperature. This is due to the recirculation which brings the molecules close again to the exit of the reactor outlet that is characterized by higher temperatures (see Figure S.9 in SI). This higher temperature is accompanied by a rise in both forward and backward reaction rates, and the rate of the backward reactions is slightly higher than for the forward reactions. However, we do not observe a drop in NO_x concentration in Figure 9, because the reaction rates are too low, as the gas temperature is only ~2000 K at maximum. Nevertheless, this second temperature peak results in a (small) drop in NO concentration, while the NO_2 concentration slightly rises (see Figure S.10 in SI). Indeed, this temperature is high enough for the conversion of NO to NO_2, but not high enough for the reverse reaction, as NO_2 is more stable than NO. However, as shown in Figure S.10, the effect is small (increase/decrease in concentration by only 0.08%), and it does not affect the total NO_x concentration. Finally, after this second temperature peak, the molecules leave the effusion nozzle, and the temperature drops further, to such low values that both forward and backward reactions are negligible and the NO_x concentration further remains constant.

For the RGA without the effusion nozzle (Figure 10b), we see the same behavior as with the nozzle, up to when the gas exits the plasma. At this stage, the gas cools down much more slowly than with the effusion

nozzle (cf. Figure 11b vs 11a). Indeed, the effusion nozzle acts as heat sink; see Figure 6 above. During this cooling, the total backward reaction rate is again higher than the total forward reaction rate, but importantly, both rates drop more slowly than for the RGA with effusion nozzle, due to the slower temperature drop. As a result, the higher total backward reaction rate is more significant than for the RGA with effusion nozzle, which explains the larger drop in the NO_x concentration in Figure 9, and thus also the lower NO_x concentration in this temperature group in Figure 8.

In summary, the effusion nozzle acts as heat sink once the molecules collide with it, causing a fast drop in temperature which "freezes" the gas composition. Hence, the backward reactions of the Zeldovich mechanism, i.e., recombination of NO with N and O atoms into N_2 and O_2, which occur at somewhat higher rate than the forward reactions, become rapidly negligible. We showed this behavior in detail for the 3750 K group, but the same was observed for the other high temperature groups (that contribute to NO_x production). This explains the slightly higher NO_x concentrations observed experimentally with the effusion nozzle. In addition, because the effusion nozzle allows ignition and sustainment of a stable plasma at slightly lower power, the (same or slightly higher) NO_x formation occurs at lower plasma power, explaining the lower energy cost, observed experimentally.

Knowing that the effusion nozzle enhances the NO_x production by removing heat from the gas and quenching the backreactions, its shape could be subjected to reactor design optimization to maximize this effect. A possible approach would be to increase the contact area between the metal and the gas by adding more radial holes to the nozzle and making these holes smaller. This way the surface-to-volume ratio of the nozzle increases, increasing the number of collisions between gas molecules and the nozzle wall and thus increasing the heat transfer. Another approach would aim to change the material of the nozzle, to maximize the heat conductivity and heat capacity of the metal, so that more heat can be absorbed by the nozzle.

5. Conclusion

Plasma-based NO_x production is gaining increasing interest as a sustainable N_2 fixation process, but the energy cost is not yet competitive with the combined Haber-Bosch and Ostwald process [9]. Hence, efforts are needed to improve the performance of plasma-based NO_x production. We present here a novel design, called "effusion nozzle", to improve the performance of an RGA plasma reactor for NO_x production. We performed experiments in a wide range of applied power, gas flow rates and N_2/O_2 ratios, and our results indicate an enhancement in NO_x concentration by 8%, as well as a reduction in energy cost by 22.5%. In absolute terms, we obtain NO_x concentrations up to 5.9%, at an energy cost down to 2.1 MJ/mol, which to our knowledge are the best values obtained up to now in atmospheric pressure plasmas. Note that we have also tested more conventional cooling options of the outflowing gas after the plasma reactor, but they did not improve the performance. The reason is that the cooling happened too late, after the recombination reactions had occurred already, as could also be explained by our modeling work. Hence, the strength of our effusion nozzle is the immediate and fast cooling right at the end of the plasma, yielding a temperature drop of almost 3500 K, and therefore avoiding the recombination reactions. This makes it superior to other, more conventional cooling options.

To understand why the effusion nozzle yields improved performance, we developed a modelling strategy, consisting of four complementary models, i.e., (i) a turbulent gas flow model, (ii) a fully-coupled heat transfer model, (iii) streamline integration, and (iv) a quasi-1D plasma chemistry model.

Our models can explain the improved performance of the effusion nozzle observed experimentally, even though we do not reach complete agreement with the measured NO_x concentrations. Indeed, our models reveal that fast cooling (quenching) occurs as soon as the gas molecules collide with the effusion nozzle, which acts as very efficient heat sink. This fast drop in temperature limits the recombination of NO with N and O atoms into N_2 and O_2, i.e., the backward reactions of the so-called Zeldovich mechanism, and thus it limits the drop in NO_x concentration after the plasma, which is much more pronounced without the effusion

nozzle, due to the slow drop in temperature after the plasma. Hence, this explains the higher NO_x concentrations observed experimentally in case of the effusion nozzle. Furthermore, because the effusion nozzle allows ignition and sustainment of the plasma at somewhat lower power, still producing the same (or even slightly higher) NO_x concentrations, this also explains the lower energy cost which was observed experimentally.

The insights obtained by this detailed analysis are not only useful to explain the better performance of the effusion nozzle, but can also help us in further improving plasma-based NO_x production, not limited to this RGA or other GA plasmas, but also other plasma types. First of all, our simulations clearly reveal that the higher temperature groups mainly contribute to NO_x formation, so a higher plasma power may cause a further rise in NO_x production, but only if the NO_x production rises faster than the power, because otherwise it would negatively affect the energy cost. Second, and even more important, the obtained insights on the effect of quenching on the detailed chemistry of the Zeldovich mechanism are very useful for designing new nozzles or other quenching options (like an additional gas or liquid flow), that can lead to fast cooling of the gas after leaving the plasma, and thus avoiding the back reactions.

Acknowledgments

This research was supported by the Excellence of Science FWO-FNRS project (FWO grant ID GoF9618n, EOS ID 30505023), the European Research Council (ERC) under the European Union's Horizon 2020 research and innovation programme (grant agreement No 810182 – SCOPE ERC Synergy project), and through long-term structural funding (Methusalem). The calculations were performed using the Turing HPC infrastructure at the CalcUA core facility of the Universiteit Antwerpen (UAntwerpen), a division of the Flemish Supercomputer Center VSC, funded by the Hercules Foundation, the Flemish Government (department EWI) and the UAntwerpen.

References

[1] N. Cherkasov, A.O. Ibhadon, P. Fitzpatrick, Chem. Eng. Process. Process Intensif. 90 (2015) 24–33.

[2] C. Smith, A.K. Hill, L. Torrente-Murciano, Energy Environ. Sci. 13 (2020) 331–344.

[3] H. Liu, Cuihua Xuebao/Chinese J. Catal. 35 (2014) 1619–1640.

[4] Y. Hou, G.L. Velthof, O. Oenema, Glob. Chang. Biol. 21 (2015) 1293–1312.

[5] J. Clemens, S. Bergmann, R. Vandré, Environ. Technol. (United Kingdom) 23 (2002) 429–435.

[6] A. Bogaerts, E.C. Neyts, ACS Energy Lett. 3 (2018) 1013–1027.

[7] R. Snoeckx, A. Bogaerts, Chem. Soc. Rev. 46 (2017) 5805–5863.

[8] J. Li, S. Yao, Z. Wu, J. Phys. D. Appl. Phys. 53 (2020).

[9] K.H.R. Rouwenhorst, F. Jardali, A. Bogaerts, L. Lefferts, Energy Environ. Sci. 14 (2021) 2520–2534.

[10] K. Birkeland, Trans. Faraday Soc. 2 (1906) 98–116.

[11] S. Eyde, J. Ind. Eng. Chem. 4 (1912) 771–774.

[12] J. Krop, I. Pollo, Chemia 678 (1981) 51–59.

[13] T. Namihira, S. Katsuki, R. Hackam, H. Akiyama, K. Okamoto, IEEE Trans. Plasma Sci. 30 (2002) 1993–1998.

[14] W. Bian, X. Song, J. Shi, X. Yin, J. Electrostat. 70 (2012) 317–326.

[15] B. Mutel, O. Dessaux, P. Goudmand, Rev. Phys. Appliquée 19 (1984) 461–464.

[16] T. Kim, S. Song, J. Kim, R. Iwasaki, Jpn. J. Appl. Phys. 49 (2010).

[17] S.G.V. Azizov R.I., Zhivotov V.K., Krotov M.F., Rusanov V.D., Tarasov Yu.V., Fridman A.A., High Energy Chem. 14 (1980) 366.

[18] S. Kelly, A. Bogaerts, Joule 5 (2021) 3006–3030.

[19] B.S. Patil, N. Cherkasov, J. Lang, A.O. Ibhadon, V. Hessel, Q. Wang, Appl. Catal. B Environ. 194

(2016) 123–133.

[20] E. Vervloessem, Y. Gorbanev, A. Nikiforov, N. De Geyter, A. Bogaerts, Green Chem. 24 (2022) 916–929.

[21] B.S. Patil, F.J.J. Peeters, G.J. van Rooij, J.A. Medrano, F. Gallucci, J. Lang, Q. Wang, V. Hessel, AIChE J. 64 (2018) 526–537.

[22] W. Wang, B. Patil, S. Heijkers, V. Hessel, A. Bogaerts, ChemSusChem 10 (2017) 2110.

[23] E. Vervloessem, M. Aghaei, F. Jardali, N. Hafezkhiabani, A. Bogaerts, ACS Sustain. Chem. Eng. 8 (2020) 9711–9720.

[24] F. Jardali, S. Van Alphen, J. Creel, H. Ahmadi Eshtehardi, M. Axelsson, R. Ingels, R. Snyders, A. Bogaerts, Green Chem. 23 (2021) 1748–1757.

[25] E. Vervloessem, M. Aghaei, F. Jardali, N. Hafezkhiabani, A. Bogaerts, ACS Sustain. Chem. Eng. 8 (2020) 9711–9720.

[26] P.R. Ammann, R.S. Timmins, AIChE J. 12 (1966) 956–963.

[27] B.S. Patil, Q. Wang, V. Hessel, J. Lang, Catal. Today 256 (2015) 49–66.

[28] S. Van Alphen, F. Jardali, J. Creel, G. Trenchev, R. Snyders, A. Bogaerts, Sustain. Energy Fuels 5 (2021) 1786–1800.

[29] F.R. Menter, AIAA 23rd Fluid Dyn. Plasmadynamics, Lasers Conf. 1993 (1993).

[30] L.C.P. S. Pancheshnyi, B. Eismann, G.J.M. Hagelaar, Univ. Toulouse, LAPLACE, CNRS-UPS-INP, Toulouse, Fr. (2008).

[31] A. Fridman, Plasma Chemistry, Cambridge University Press, Cambridge, U.K., 2008.

[32] C.J. Dawson, J. Hilton, Food Policy 36 (2011) S14–S22.